

Viscosity of Earth's Outer Core[†]

D. E. SMYLIE¹ and Andrew Palmer²

¹Department of Earth and Space Science and Engineering, York University
4700 Keele Street, Toronto, Ontario, M3J 1P3, CANADA
Phone:(416) 736-2100, ext. 66438, Fax:(416) 736-5817
E-mail: doug@core.yorku.ca

²Department of Physics and Astronomy, York University
4700 Keele Street, Toronto, Ontario, M3J 1P3, CANADA
E-mail: palmer@core.yorku.ca

Abstract

A viscosity profile across the entire fluid outer core is found by interpolating between measured boundary values, using a differential form of the Arrhenius law governing pressure and temperature dependence. The discovery that both the retrograde and prograde free core nutations are in free decay (Palmer and Smylie, 2005) allows direct measures of viscosity at the top of the outer core, while the reduction in the rotational splitting of the two equatorial translational modes of the inner core allows it to be measured at the bottom. We find $2,371 \pm 1,530 \text{ Pa} \cdot \text{s}$ at the top and $1.247 \pm 0.035 \times 10^{11} \text{ Pa} \cdot \text{s}$ at the bottom.

Following Brazhkin (1998) and Brazhkin and Lyapin (2000) who get $10^2 \text{ Pa} \cdot \text{s}$ at the top, $10^{11} \text{ Pa} \cdot \text{s}$ at the bottom, by an Arrhenius extrapolation of laboratory experiments, we use a differential form of the Arrhenius law to interpolate along the melting temperature curve to find a viscosity profile across the outer core. We find the variation to be closely log-linear between the measured boundary values.

The close agreement of the boundary values of viscosity, found by Arrhenius extrapolation of laboratory experiments, with those found from the free core nutations, and the inner core translational modes, suggests that core flows are laminar and that the returned viscosities are measures of their molecular values. This would not be the case in the presence of the vigorous turbulent convection sometimes postulated by dynamo theorists.

The local Ekman number is found to range from 10^{-2} at the bottom of the outer core to 10^{-10} at the top. Except in the very lower part of the outer core, Ekman numbers are in the range 10^{-4} to 10^{-5} , or below, in which the laminar flows of numerical dynamos and laboratory rotating fluids experiments occur.

We find explicit expressions for the reciprocal Q 's at both boundaries and for the viscous coupling torques between the outer core and shell, and between the outer and inner cores. For the high viscosity in the F-layer outside the ICB found from the reduction in the rotational splitting of the two equatorial translational modes of the inner core, the inner core is found to be tightly coupled to the outer core with a negligible contribution to dissipation in the free core nutation modes.

[†]Published electronically in arXiv.org>physics >physics.geo-ph, Cornell University Library, Ithaca, N. Y., August 2, 2018.

1 Introduction

Properties of Earth's deep interior, such as its elasticity, density, pressure and gravity have traditionally been obtained through the inversion of seismic observations. While these have been important to our understanding of Earth's internal structure, the viscosity of the outer fluid core is crucial to our understanding of its dynamics and the generation of the geomagnetic field. Direct observations and limits on viscosity have traditionally been much larger than those values found on the basis of extrapolations of laboratory high pressure and temperature experiments (Lumb and Aldridge, 1991). The latter tend to be close to that of liquid iron at atmospheric pressure (Rutter et al., 2002), while the former are many orders of magnitude larger (Davis and Whaler, 1997).

Unusual properties of the lower outer core have long been suspected, going back to the 1926 claim by Jeffreys (Jeffreys, 1926) of a strong negative P-wave velocity gradient there. While the P gradient is now thought to be small, but slightly positive, possibly due to solid inclusions slowing compressional waves in that region (Garland, 1971, pp.42-50), its properties remain a subject of speculation. A new seismic phase, PKhKP, has even been suggested by Bolt (Bullen and Bolt, 1985, p.317) as originating from reflections in the lower outer core.

With the discovery that both the retrograde and prograde free core nutations are in free decay (Palmer and Smylie, 2005), direct measures of the viscosity at the top of the outer core can be made. In this paper, we present a detailed analysis of both the Ekman layer at the top of the outer core and that at the bottom, just outside the inner core boundary. Our analysis yields a mean value of $2,371 \pm 1,530 Pa \cdot s$ for the recovered dynamic viscosity at the top of the outer core. From the reduction in the rotational splitting of the two equatorial translational modes of the inner core, two independent measures of viscosity in the F-layer at the bottom of the outer core are found (Smylie, 1999; Smylie and McMillan, 2000), as the reduction is larger for the retrograde mode than for the prograde mode. The retrograde equatorial mode gives $1.190 \pm 0.035 \times 10^{11} Pa \cdot s$, while the prograde equatorial mode gives $1.304 \pm 0.034 \times 10^{11} Pa \cdot s$ for an average value of $1.247 \pm 0.035 \times 10^{11} Pa \cdot s$.

Our values of viscosity at the boundaries of the outer core are in close agreement with an Arrhenius extrapolation of laboratory experiments by Brazhkin (1998) and by Brazhkin and Lyapin (2000) who find $10^2 Pa \cdot s$ at the top of the outer core and $10^{11} Pa \cdot s$ at the bottom. Although the Arrhenius model is widely used over the limited ranges of pressure and temperature involved in laboratory experiments (Dobson, 2002), its exponential nature yields values of viscosity that appear extreme when extrapolated from laboratory pressures of the order of $30 GPa$ by more than a factor of ten to outer core pressures, and when the temperature extrapolation from laboratory values of the order of $2,000 K$ is by a factor of two to outer core melting temperatures. Our measured viscosities at the boundaries appear to confirm the validity of Arrhenius extrapolation.

The close agreement of the boundary values of viscosity with an Arrhenius extrapolation of laboratory experiments prompts us to construct a viscosity profile across the entire outer core using the Arrhenius law. Due to the strong pressure dependence of the activation volume, it is necessary to use a differential form of the Arrhenius law to interpolate along the melting temperature curve between the measured boundary values of viscosity.

Both the free core nutations and the translational oscillations of the inner core are highly influenced by Earth's rotation. They are examples of dynamical phenomena in contained rotating fluids. This is a subject that was of much interest several decades ago based on the inertial wave equation (Stewartson and Roberts, 1963; Roberts and Stewartson, 1965; Greenspan, 1969; Busse, 1968; Aldridge and Toomre, 1969). In these descriptions, the container rotation is constrained

rather than free, there is no inner body, the fluid is assumed incompressible, uniform and non self-gravitating and the container is taken to be rigid. Although the theories were beautifully confirmed by laboratory experiments (Aldridge, 1967) their relevance to the real Earth in which the rotation of the container is unconstrained, there is an inner body, the fluid is compressible, stratified and self-gravitating and the boundaries are deformable does not appear to be direct. The governing equation then becomes the subseismic wave equation rather than the inertial wave equation (Smylie, Jiang, Brennan and Sato, 1992). The free core nutations are solutions of the subseismic wave equation which are close to pure rotations with respect to the shell, though not exactly so (Jiang, 1993; Jiang and Smylie, 1995; Jiang and Smylie, 1996). Thus, the motions in the Earth frame imitate the ‘spin-over’ mode of the inertial wave equation. Some of the basic features of the Ekman layers at the two boundaries in the real Earth resemble those of the ‘spin-over’ mode but previous theories are not given in detail with only results shown, possibly due to Greenspan’s dictum that the ‘computation of viscous effects, ..., is laborious but straightforward’ (Greenspan, 1969, p.66). We give full details of the analysis of the Ekman layers at the two boundaries independent of the inertial wave equation, and calculate in detail the viscous coupling between the outer and inner cores and the shell in two Appendices. These details appear not to have been published previously. Explicit expressions are obtained for the reciprocal Q ’s at both boundaries, and for the viscous coupling torques between the outer core and the shell (mantle plus crust), and between the outer and inner cores. The inner core is found to be tightly coupled by viscosity to the outer core in the free core nutations.

While the variational calculations of Jiang (1993) showed that there should be a prograde free core nutation (PFCN), in addition to the classical retrograde free core nutation (RFCN), he was anticipated in this discovery by both Mathews et al (1991), and by de Vries and Wahr (1991), in studies of the response of the Earth to nutational forcing. At the time, the VLBI nutation record was too short to give an acceptable confidence level, and no claim of observational support was made.

There has been much interest in the detection of the inner core translational triplet of modes in the spectra of superconducting gravimeter observations since the initial identification fifteen years ago. They were first identified visually in the Product Spectrum of a total of 110,000 hours of observations at four European stations (see Figure 9 of Smylie, Jiang, Brennan and Sato, 1992). By adjustment of the degree one internal load Love numbers, they were quickly shown to have the correct splitting to be the translational triplet. A more complete study was made by Smylie, Hinderer, Richter and Ducarme (1993), including a complete analysis of the statistics of the Product Spectrum and a search across 4,119 frequencies for correctly split triplets in the subtidal band between $2hr$ and $8hr$. The details of this search are summarized in Section 3 of the present paper. It was shown that the triplet originally identified visually had only one chance in 6.8×10^{38} of being random. Nonetheless, the original identification generated a flurry of papers, pro and con, on this result. Hinderer, Crossley and Jensen (1995) were able to confirm the earlier result in the Product Spectrum of the same data sets, although by a different spectral analysis technique. Smylie, Hinderer, Richter and Ducarme (1993) had used the Welch Overlapping Segment Analysis (WOSA) method, in which 12,000 hr segments, windowed with a Parzen window with 75% overlap, enabled an improved signal to noise ratio. In this case, the variance is inflated by a factor of 1.5 but the record length is quadrupled, for an overall increase in effective record length of $8/3$. Hinderer, Crossley and Jensen (1995) were unable to find the triplet in the cross spectrum of two years of common observations at just two stations, Cantley, Canada and Strasbourg, France. They had hoped for an improved result, even though simultaneous, short records from only two stations were

used, because the cross spectrum takes phase information into account.

Apart from the difficulties associated with the low signal to noise ratio of the translational resonances in the spectra of superconducting gravimeter observations, a second source of confusion is the calculation of the translational mode periods for a given Earth model. Most calculations use truncated vector spherical harmonic expansions derived from normal mode theory (Rogister, 2003). The problem with this approach is that the Coriolis acceleration couples these modes into slowly convergent infinite chains. Typically, these infinite chains are truncated after only a few terms. Johnson and Smylie (1977) showed that at periods of hours and more, convergence is very slow and that many terms need to be included for accurate computation of periods. This led Smylie, Jiang, Brennan and Sato (1992) to develop a variational, finite element method of computing long period core modes using bicubic splines as support functions. This method was used in the calculation of translational mode periods and was extended by Jiang (1993) to determine solutions for the free core nutations. The finite element method, using local basis functions rather than global spherical vector harmonics, avoids the Coriolis coupling problem and allows the accurate calculation of periods. The initial formulation was criticized by Crossley, Rochester and Peng (1992) on the grounds that dynamical terms arising from pure translations had been neglected. This shortcoming was easily corrected (Smylie and Jiang, 1993). They showed that the degree one reciprocal Love number for the inner core has a quadratic dependence on frequency, as illustrated in Figure 5 of that paper. This shortcoming did not affect the original identification of the translational triplet, and current computations take the frequency dependence of Love numbers, used to describe the deformations of the shell (mantle and crust) and inner core, fully into account. The inviscid translational mode periods for four Earth models are tabulated in Table 2, and are used in the splitting law plot shown in Figure 6. The computation of these periods is now done routinely to six or seven significant figures.

Nonetheless, there remains a wide range of quoted translational triplet periods in the literature. Crossley, Rochester and Peng (1992) give the triplet for Earth model 1066A as (4.04970, 4.43806, 4.89647) hours, close to the known values in Table 2 of (4.0491, 4.4199, 4.8603) hours. The next year, Crossley (1993) found (4.127, 4.533, 5.016) hours, while Rogister (2003), using normal mode theory, got (4.129, 4.529, 5.024) hours. Similarly, Rosat, Rogister, Crossley and Hinderer (2006) quote (4.64776, 5.24395, 5.83488) hours and (4.74744, 5.35865, 5.92142) for Earth model PREM, compared to the known triplet (4.6776, 5.1814, 5.7991) hours in Table 2. The noise level of quoted periods in the literature, even among papers with common authors, seems to exceed the noise level in the spectra of superconducting gravimeter observations by a large margin! While the scatter of reported periods may be due to attempts to apply truncated normal mode theory, the situation was complicated, even further, by Rieutord (2002) who finds (3.894, 4.255, 4.687) hours for Earth model 1066A. He misquotes the periods of Crossley, Rochester and Peng (1992) as (4.95, 4.438, 4.896) hours. The divergence of Rieutord's periods from known values, apart from typographical errors, appears to be due to his assumption that the shell (mantle and crust) and inner core are perfectly rigid, and that the fluid outer core is perfectly adiabatically stratified. He further dismisses the measurement of viscosity by Smylie and McMillan (2000), from the reduction of rotational splitting of the two equatorial translational modes, on the grounds that second order Ekman boundary layer theory is required, even though he fails to perform the required second order analysis to support this claim. For the observed Ekman number of 1.2×10^{-2} , since the Ekman layer theory is an ascending series in the square root of the Ekman number, second order theory would give a correction of 0.11 or 11%. The two independent measures of viscosity from the two

equatorial modes differ by 9.6%. It is not known if this difference is due to the neglect of second order terms in the Ekman boundary layer theory.

The most comprehensive analysis of superconducting gravimeter observations appears to be that of Courtier et al (2000). A total of 294, 106 hours were assembled for analysis. In addition to Product Spectra, a global multistation experiment was performed using simultaneous observations from Brussels, Cantley, Kakioka, Strasbourg and Wuhan, allowing the use of phase to lower noise levels. Four independent sets of translational mode periods were recovered, including those shown in Figure 3 of the present paper, all differing from the original identification by no more than in the fifth significant figure. A similar global experiment using the Product Spectrum was attempted by Kroner, Jahr and Jentzsch (2004) for observations at five stations without result. Insufficient detail is given to determine if the data sets were correctly windowed to prevent frequency mixing from finite record effects, but the presence of tidal lines in the subtidal band suggests not. Also the inclusion of the Boulder data set, which has known serious timing errors, may have compromised the results. Finally, little is known about the excitation of the translational modes. Like the free core nutations, they may not be continuously excited, and may not be present in more recent observations.

By contrast, a recent new development in the search for the translational modes has been achieved by Pagiatakis, Yin and El-Gelil (2007). Instead of using the Product Spectrum based on 12, 000 hour segments, across many stations, they use only the Cantley record of seventy-two months length. For each month they compute a least squares periodogram. Then, in a variation of the Product Spectrum method, they use the geometric mean of the seventy-two periodograms to look for translational modes. While the use of only one month data segments limits resolution, they find support for the periods found in the original detection using the Product Spectrum.

As illustrated in Figure 7, the translational mode periods are very sensitive to inner core density. From Table 3, we see that the Cal8 Earth model of Bolt and Uhrhammer gives periods very close to those observed. A reduction of only $2.25 \text{ milligrams} \cdot \text{cm}^{-3}$ in inner core density brings the three periods for this Earth model into coincidence with the observed triplet (Smylie, Francis and Merriam, 2001). In terms of the density jump at the inner core boundary, the Cal8 value of $1, 170 \text{ kg} \cdot \text{m}^{-3}$ is reduced to $1, 168 \text{ kg} \cdot \text{m}^{-3}$.

Traditionally, the dichotomy between extrapolated laboratory values of viscosity and directly observed values for the Earth's core (Lumb and Aldridge, 1991), the latter being many orders of magnitude larger, has been explained by dynamo theorists as due to turbulent flow, with the observed values reflecting eddy viscosities. It is difficult to see how turbulent flow could explain observed viscosities spanning nearly eight orders of magnitude across the core. This view is also challenged by the close agreement of our measured boundary values with the Arrhenius extrapolation of laboratory experiments by Brazhkin (1998) and by Brazhkin and Lyapin (2000). The latter reflect molecular viscosities. While turbulent flow may enhance dynamo action, successful numerical dynamos with laminar flow, and with Ekman numbers in the range implied by our measured viscosities have been routinely achieved (Olsen and Christiansen, 2002).

2 Viscosity at the Top of the Outer Core

In realistic Earth models, the finite element-based variational calculations of Jiang (1993) showed that there are two free core nutations. In addition to the classical retrograde mode (RFCN), a second prograde mode (PFCN) appears. The motions are illustrated by Poincaré constructions, in which a

small body cone rolls once per sidereal day without slipping on a large space cone as shown Figure 1 below.

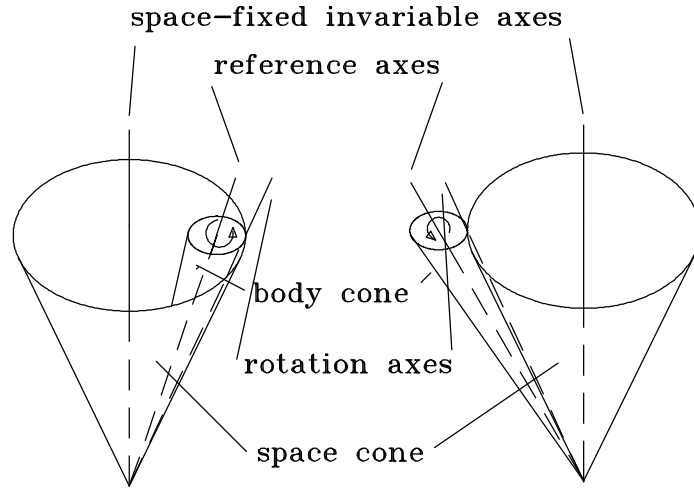


Figure 1: Poincaré constructions for the Free Core Nutations. The RFCN is shown on the left, the PFCN on the right. In each mode, the small body cone rolls once per sidereal day without slipping on the large space cone. The line of contact is Earth's instantaneous rotation axis.

In the Earth frame, both modes appear as nearly diurnal retrograde wobbles, the wobble associated with the RFCN is a little faster than retrograde diurnal, while the wobble associated with the PFCN is a little slower. For the RFCN, the ratio of the nutation amplitude a_N to the wobble amplitude a_W is given by $a_N/a_W - 1 = -\Omega/\sigma_N$, where Ω is Earth's angular rotation velocity and σ_N is the nutation angular frequency. For the PFCN, the ratio is given by $a_N/a_W + 1 = \Omega/\sigma_N$.

In the study of Palmer and Smylie (Palmer and Smylie, 2005), both the RFCN and the PFCN were found to be in free decay, on the basis of VLBI nutation measurement series from GSFC and the USNO in excess of twenty-three years length. The GSFC series runs from August 3, 1979 to March 6, 2003 and is taken to span a period of 8,617 days, while the USNO series runs from August 3, 1979 to March 29, 2003 and is taken to span 8,631 days. In order to investigate the decays in detail, each record was divided into 2,000 day segments, advancing down the time axis in 400 day steps. Spectral densities were estimated on the basis of each of four successive 2,000 day segments. The result was spectral estimates centered at 1,600 days into the record, and at 400 day increments down the time axis thereafter. The spectral amplitudes are shown plotted against time in Figure 2.

In free decay, the logarithm of the nutation amplitude a_N decreases linearly with time and

$$\log a_N = ct + d, \tag{1}$$

with

$$c = \pm \frac{\pi \log e}{Q_N T_N} = -\frac{\log e}{\tau}, \quad d = \log a_{N_0}, \tag{2}$$

$$t_{1/2} = \tau \ln 2, \tag{3}$$

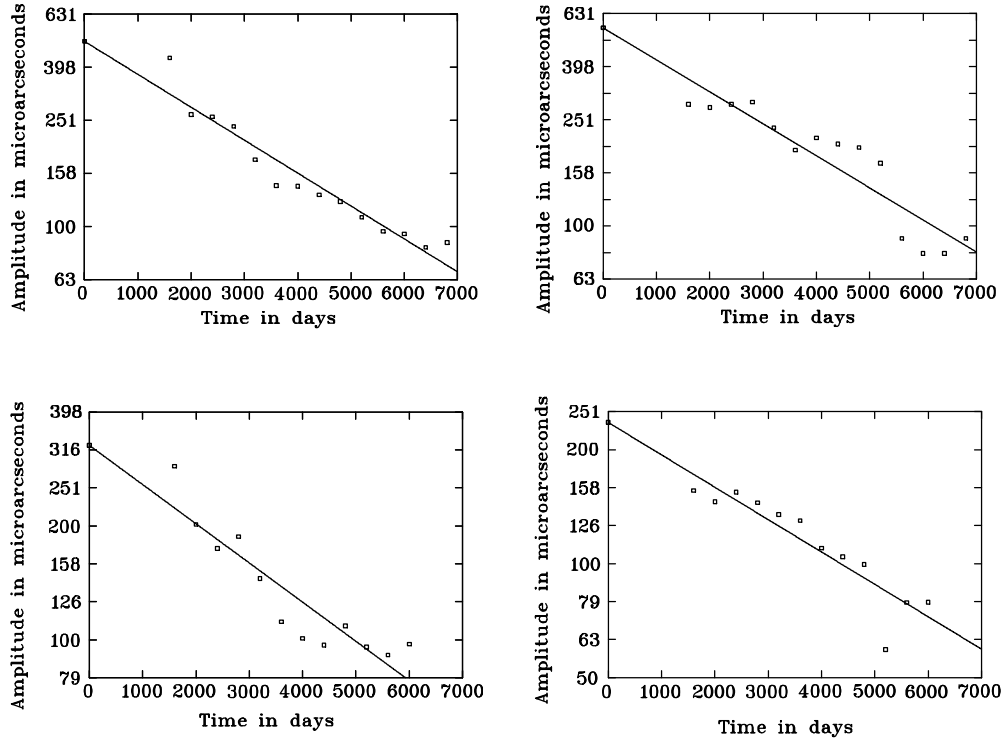


Figure 2: Amplitudes of the free core nutations plotted on a logarithmic scale as functions of time. Upper plots show the RFCN, upper left for GSFC, upper right for USNO, lower plots show the PFCN, lower left for GSFC, lower right for USNO. Linear fits to the time dependencies are shown directly on the plots, along with extrapolated values at the time origin.

where T_N is the signed nutation period (negative for retrograde, positive for prograde), Q_N is the apparent Q of the nutation in the space frame, a_{N_0} is the amplitude at time $t = 0$, τ is the e-folding time and $t_{1/2}$ is the half life of the decay. The upper positive sign applies to the RFCN, while the lower negative sign applies to the PFCN.

The actual physical dissipation takes place in the Earth frame, through the associated nearly diurnal retrograde wobbles, and is measured by Q_W . Q_W is related to the apparent nutation Q by

$$Q_W = \pm (1 - T_N/T_s) Q_N, \quad (4)$$

with T_s being the length of the sidereal day. The wobble Q is found to be

$$Q_W = -\frac{\pi \log e}{cT_s} (1 - T_s/T_N). \quad (5)$$

Results of the regression on the logarithm of the nutation amplitude, (1), are given in Table 1.

In realistic Earth models, the two free core nutations have associated nearly diurnal retrograde wobbles that are close to pure rotations with respect to the shell (mantle and crust) and the inner core (Jiang, 1993; Jiang and Smylie, 1995; Jiang and Smylie, 1996). Their angular frequencies are close to $-\Omega$, the negative of Earth's angular rotation velocity. In spherical polar co-ordinates (r, θ, ϕ) the velocity field is closely

$$\mathbf{v} = -\hat{\theta} A r \sin(\phi + \Omega t) - \hat{\phi} A r \cos \theta \cos(\phi + \Omega t), \quad (6)$$

Table 1: Fitted decay parameters of the Free Core Nutations.

		c (10^{-4}days^{-1})	d	a_{N_0} (μas)	T_N (days)	Q_N	Q_W	$t_{1/2}$ (days)
RFCN								
	GSFC	-1.23909 ± 0.1006	2.69740	498.20	-440.865 ± 31.519	26.404 ± 4.031	11,068 $\pm 2,481$	2,429
	USNO	-1.20360 ± 0.1486	2.74547	556.51	-410.147 ± 17.706	27.444 ± 4.573	11,394 $\pm 2,390$	2,501
PFCN								
	GSFC	-1.03217 ± 0.1461	2.51192	325.03	474.308 ± 86.578	34.052 ± 11.036	13,221 $\pm 6,698$	2,916
	USNO	-0.85237 ± 0.1236	2.37147	235.22	444.847 ± 74.677	41.356 ± 12.939	16,009 $\pm 7,696$	3,532

for nearly diurnal wobble amplitude A .

On the assumption that the boundary layers are a small fraction of the radius in thickness, the leading order boundary layer equations in the (θ, ϕ) components of the extra boundary layer velocity, (v_θ, v_ϕ) , are (Moore, 1978; Smylie and McMillan, 1998)

$$\begin{aligned} \frac{\partial v_\theta}{\partial t} - 2\Omega v_\phi \cos \theta &= \nu \frac{\partial^2 v_\theta}{\partial r^2}, \\ \frac{\partial v_\phi}{\partial t} + 2\Omega v_\theta \cos \theta &= \nu \frac{\partial^2 v_\phi}{\partial r^2}, \end{aligned} \quad (7)$$

with ν denoting the kinematic viscosity.

The detailed solution of these boundary layer equations, and the calculation of the rates of energy dissipation in each of the respective layers at the boundaries of the outer core is left to Appendix A. From equation (85) of that Appendix, the rate of energy dissipation in each of the respective boundary layers is found to be

$$\frac{dE}{dt} = \frac{\pi}{35} \rho_0 A^2 r_0^4 \sqrt{2\nu\Omega} (9\sqrt{3} + 19) \quad (8)$$

with ρ_0 denoting the density, A the amplitude, and r_0 the radius at the boundaries. If A_a is the amplitude of the nearly diurnal retrograde wobble of the outer core with respect to the inner core, and if A_b is the amplitude with respect to the shell, the total energy dissipated per cycle in both boundary layers is

$$E = \frac{2\pi}{\Omega} \cdot \frac{dE}{dt} = \frac{2}{35} \pi^2 (\rho_0(a) A_a^2 a^4 \sqrt{\nu_a} + \rho_0(b) A_b^2 b^4 \sqrt{\nu_b}) \sqrt{\frac{2}{\Omega}} (9\sqrt{3} + 19), \quad (9)$$

with $\rho_0(a)$ and ν_a representing the density and kinematic viscosity just outside the ICB (at $r_0 = a$) and $\rho_0(b)$ and ν_b representing the density and kinematic viscosity just inside the CMB (at $r_0 = b$). The quality factor of the nearly diurnal wobbles accompanying the free core nutations, Q_W , is defined as 2π times the ratio of the total energy to the energy dissipated per cycle, E . The total energy of the motion is closely

$$\frac{1}{2} I_{oc} A^2, \quad (10)$$

where $I_{oc} = 911.79 \times 10^{34} \text{ kg} \cdot \text{m}^2$ is the moment of inertia of the outer core. The reciprocal of the overall quality factor is then the sum of the reciprocals of the effective quality factors at the two boundaries,

$$\frac{1}{Q_W} = \frac{1}{Q_a} + \frac{1}{Q_b}, \quad (11)$$

with

$$\frac{1}{Q_a} = \frac{2\pi\rho_0(a)a^4\sqrt{2\nu_a/\Omega}(9\sqrt{3}+19)}{35I_{oc}}, \quad (12)$$

$$\frac{1}{Q_b} = \frac{2\pi\rho_0(b)b^4\sqrt{2\nu_b/\Omega}(9\sqrt{3}+19)}{35I_{oc}}. \quad (13)$$

Neglecting the perturbation on shell rotation, if the amplitude of the nearly diurnal wobble of the outer core is B and that of the inner core is C ,

$$A_b = B, \quad A_a = B - C.$$

The detailed calculation of the viscous coupling torques the outer core exerts on the shell and inner core is left to Appendix B. From expressions (103) and (104) of that Appendix, and ignoring the small Chandler resonance effect, the equation of motion of the outer core is

$$\gamma_a e^{-i\Omega t} (C - B) - \gamma_b e^{-i\Omega t} B = I_{oc} (\dot{B} - i\Omega B) e^{-i\Omega t}, \quad (14)$$

while that of the inner core is

$$-\gamma_a e^{-i\Omega t} (C - B) = I_{ic} (\dot{C} - i\Omega C) e^{-i\Omega t}, \quad (15)$$

with I_{ic} representing the moment of inertia of the inner core. Equations (14) and (15) constitute a linear, homogeneous differential system. For time dependence $e^{\lambda t}$, it becomes

$$\begin{pmatrix} \lambda - i\Omega + (\gamma_a + \gamma_b)/I_{oc} & -\gamma_a/I_{oc} \\ -\gamma_a/I_{ic} & \lambda - i\Omega + \gamma_a/I_{ic} \end{pmatrix} \begin{pmatrix} B \\ C \end{pmatrix} = 0, \quad (16)$$

with characteristic equation

$$\lambda'^2 + \left(\frac{1 + \gamma_b/\gamma_a}{I_{oc}} + \frac{1}{I_{ic}} \right) \gamma_a \lambda' + \frac{\gamma_a \gamma_b}{I_{oc} I_{ic}} = 0, \quad (17)$$

where $\lambda' = \lambda - i\Omega$.

From (103), (104), the ratio

$$\frac{\gamma_b}{\gamma_a} = \frac{\rho_0(b)b^4\sqrt{\nu_b}}{\rho_0(a)a^4\sqrt{\nu_a}} = 1/117.4, \quad (18)$$

for density ratio 0.8069, radius ratio 2.8668, and the ratio of the square roots of the kinematic viscosities 1/6400. Correct to terms of first order in the small quantity γ_b/γ_a , the roots of the characteristic equation are

$$\lambda'_1 = \frac{\gamma_b}{I_c}, \quad \text{and} \quad \lambda'_2 = -\frac{I_c}{I_{oc}I_{ic}}\gamma_a - \frac{I_{ic}}{I_{oc}I_c}\gamma_b, \quad (19)$$

with $I_c = I_{oc} + I_{ic}$ representing the moment of inertia of the entire core. The admissible solutions of the system (16) are then the linear combinations

$$\begin{aligned} B e^{-i\Omega t} &= \alpha e^{\lambda_1 t} + \beta e^{\lambda_2 t}, \\ C e^{-i\Omega t} &= \left(1 + \frac{\gamma_b I_{ic}}{\gamma_a I_c}\right) \alpha e^{\lambda_1 t} - \left(\frac{I_{oc}}{I_{ic}} - \frac{\gamma_b I_{oc}}{\gamma_a I_c}\right) \beta e^{\lambda_2 t}, \end{aligned} \quad (20)$$

with α, β representing arbitrary linear combination coefficients. The decay times of the two solutions are, respectively

$$\tau_1 = \frac{I_c}{Rl\gamma_b}, \quad (21)$$

$$\tau_2 = \frac{I_{oc} I_{ic}}{(I_c Rl\gamma_a + I_{ic} Rl\gamma_b)}, \quad (22)$$

where

$$Rl\gamma_a = \pi\rho_0(a) a^4 \sqrt{v_a \Omega} \frac{\sqrt{2}}{35} [9\sqrt{3} + 19], \quad (23)$$

$$Rl\gamma_b = \pi\rho_0(b) b^4 \sqrt{v_b \Omega} \frac{\sqrt{2}}{35} [9\sqrt{3} + 19]. \quad (24)$$

Again, correct to first order in the small quantity γ_b/γ_a , the ratio of the decay times is

$$\frac{\tau_2}{\tau_1} = \frac{I_{oc} I_{ic} Rl\gamma_b}{I_c^2 Rl\gamma_a} = \frac{I_{oc} I_{ic} \gamma_b}{I_c^2 \gamma_a}. \quad (25)$$

With $I_{oc} = 911.79 \times 10^{34} \text{ kg} \cdot \text{m}^2$, $I_{ic} = 6.16 \times 10^{34} \text{ kg} \cdot \text{m}^2$ and, hence $I_c = 917.95 \times 10^{34} \text{ kg} \cdot \text{m}^2$, we have $\tau_2/\tau_1 = 1/17, 613$. Thus, the second solution damps out rapidly, and we are left with

$$C = \left(1 + \frac{\gamma_b I_{ic}}{\gamma_a I_c}\right) B, \quad (26)$$

and

$$B - C = -\frac{\gamma_b I_{ic}}{\gamma_a I_c} B. \quad (27)$$

From expression (85), the total rate of energy dissipation at both boundaries then becomes

$$\frac{dE}{dt} = \pi\rho_0(b) A_b^2 b^4 \sqrt{v_b \Omega} \frac{\sqrt{2}}{35} (9\sqrt{3} + 19) \left[1 + \frac{\gamma_b}{\gamma_a} \left(\frac{I_{ic}}{I_c}\right)^2\right]. \quad (28)$$

The energy dissipated per cycle is

$$E = \frac{2\pi}{\Omega} \cdot \frac{dE}{dt} = \frac{2}{35} \pi^2 \rho_0(b) A_b^2 b^4 \sqrt{\frac{2v_b}{\Omega}} (9\sqrt{3} + 19) \left[1 + \frac{\gamma_b}{\gamma_a} \left(\frac{I_{ic}}{I_c}\right)^2\right]. \quad (29)$$

The total energy of the motion is

$$T = \frac{1}{2} I_{oc} A_b^2 + \frac{1}{2} I_{ic} \left[1 + \frac{\gamma_b I_{ic}}{\gamma_a I_c}\right]^2 = \frac{1}{2} I_c \left[1 + 2\frac{\gamma_b}{\gamma_a} \left(\frac{I_{ic}}{I_c}\right)^2\right] A_b^2 \quad (30)$$

to first order in the small quantity γ_b/γ_a . To the same order, the wobble quality factor is

$$Q_W = 2\pi T/E = \frac{35I_c \left[1 + \gamma_b/\gamma_a (I_{ic}/I_c)^2\right]}{2\pi\rho_0(b) b^4 \sqrt{2\nu_b/\Omega} (9\sqrt{3} + 19)}. \quad (31)$$

Finally, correct to first order, the viscosity recovered from the observed Q_W of the nearly diurnal retrograde wobbles is

$$\nu_b = \frac{1225I_c^2\Omega \left[1 + 2\gamma_b/\gamma_a (I_{ic}/I_c)^2\right]}{8\pi^2\rho_0^2(b) b^8 (9\sqrt{3} + 19)^2 Q_W^2}. \quad (32)$$

We see from this expression that the inner core is tightly coupled to the outer core motion, and that the correction for dissipation in the lower boundary layer, represented by the quantity in square brackets on the numerator, differs from unity by only 3.8×10^{-7} and may be neglected.

Using expression (32), and the values of Q_W listed in Table 1, we recover a viscosity of $3,038 \pm 1,362 \text{ Pa} \cdot \text{s}$ for the RFCN from the GSFC series, $2,866 \pm 1,203 \text{ Pa} \cdot \text{s}$ from the USNO series, $2,129 \pm 2,157 \text{ Pa} \cdot \text{s}$ for the PFCN from the GSFC series and $1,452 \pm 1,396 \text{ Pa} \cdot \text{s}$ from the USNO series. The mean value of the recovered dynamic viscosity is then $2,371 \pm 1,530 \text{ Pa} \cdot \text{s}$. For a density of $9.82 \times 10^3 \text{ kg} \cdot \text{m}^{-3}$ at the top of the core, the corresponding kinematic viscosity is $0.2414 \pm 0.1558 \text{ m}^2 \text{ s}^{-1}$.

3 Viscosity at the Bottom of the Outer Core

Near the bottom of the outer core, the viscosity in the F-layer (Smylie, 1999; Smylie and McMillan, 2000) can be found from the reduction in the rotational splitting of the two equatorial translational modes of the Inner Core. The translational modes are observed in the Product Spectrum of global networks of superconducting gravimeters (Smylie, Hinderer, Richter and Ducarme, 1993; Courtier et al., 2000). In Figure 3, we show the three translational mode resonances found in the Product Spectrum, based on observations at Bad Homburg (24,272 hours), Brussels (83,892 hours), Cantley (32,992 hours) and Strasbourg (78,504 hours). Both the prograde and axial mode resonances are well above the 95% C.I. and the retrograde mode is just below this level of significance (Fig.8 (b), Courtier et al., 2000).

A much more stringent test of significance arises from consideration of the pressure and viscous drags on the Inner Core (Smylie and McMillan, 2000) which leads to a splitting law of the form

$$\left(\frac{T}{T_0}\right)^2 + 2g^v \frac{T_0}{T_s} \left(\frac{T}{T_0}\right) - 1 = 0, \quad (33)$$

where T is the period, T_0 is the unsplit period, T_s is the length of the sidereal day, and g^v is a dimensionless viscous splitting parameter. For the axial mode, the viscous splitting parameter is related to the inviscid splitting parameter g^i by

$$g^v = g^i \left[1 + \frac{1}{4} \frac{M_I - M'_I}{M_I + \alpha} \sqrt{E_k} f^a(\sigma)\right], \quad (34)$$

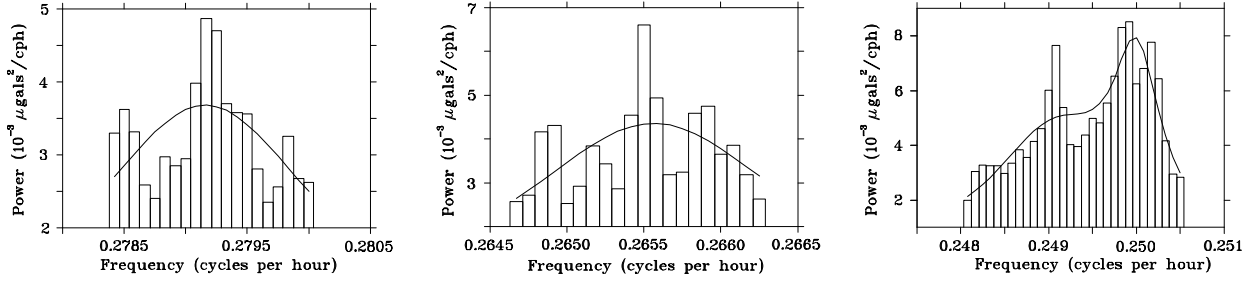


Figure 3: Product Spectra of (from left to right) the retrograde equatorial, axial and prograde equatorial translational modes of the Inner Core. The prograde equatorial mode is near the large solar heating tide feature S_6 at exactly six cycles per solar day. The recovered central periods are, respectively $3.5822 \pm 0.0012 \text{ hr}$, $3.7656 \pm 0.0015 \text{ hr}$ and $4.0150 \pm 0.0010 \text{ hr}$.

and for the equatorial modes by

$$g^v = g^i \left[1 - \frac{1}{8} \left(\frac{M'_I - \beta}{M_I + \beta} + \frac{M'_I + \alpha}{M_I + \alpha} \right) \sqrt{E_k} f^e(\sigma) \right]. \quad (35)$$

α, β are coefficients of the pressure drag on the Inner Core given by

$$\alpha = M'_I \left(\frac{1}{2} + \frac{3}{2} \frac{M_I + (a/b)^3 M_S}{M_O + M_S (1 - (a/b)^3)} \right), \quad (36)$$

and

$$\beta = M'_I \left(\frac{1}{4} - \frac{3}{4} \frac{M_I + (a/b)^3 M_S}{M_O + M_S (1 - (a/b)^3)} \right). \quad (37)$$

M_I is the mass of the Inner Core, M_O is the mass of the outer core, M_S is the mass of the shell, and $M'_I = 4/3\pi a^3 \rho_0(a)$ is the displaced mass, $\rho_0(a)$ the density at the bottom of the outer core. $\sigma = \omega/2\Omega$ is the dimensionless Coriolis frequency corresponding to angular frequency ω . $f^a(\sigma)$, $f^e(\sigma)$ are dimensionless functions of σ given by

$$f^a(\sigma) = \left\{ 8 \left[(\sigma + 1)^{3/2} + (\sigma - 1)^{3/2} \right] - \frac{16}{5} \left[(\sigma + 1)^{5/2} - (\sigma - 1)^{5/2} \right] \right\}, \quad (38)$$

and

$$f^e(\sigma) = \left\{ \mp 24 (\pm\sigma \mp 1)^{1/2} - 16 (\pm\sigma \mp 1)^{3/2} - \frac{16}{5} \left[(\pm\sigma - 1)^{5/2} - (\pm\sigma + 1)^{5/2} \right] \right\}, \quad (39)$$

with the upper sign referring to the retrograde mode, for which σ is positive and the lower sign referring to the prograde mode, for which σ is negative.

For three candidate periods, T_R (retrograde), T_C (axial) and T_P (prograde), the splitting equation (33) provides the corresponding values of the dimensionless viscous splitting parameter, g_R^v , g_C^v , and g_P^v , for a given value of T_0 . Thus, the whole frequency axis can be searched for correctly split resonances. For a resonance centred on frequency f_j , its form at neighbouring frequencies f_i is

$$r_{ij} = \frac{a_j^2}{1 + 4Q \left[(f_i - f_j) / f_j \right]^2}. \quad (40)$$

For record segments of 12,000 *hour* length, Product Spectral estimates s_i are spaced at intervals of $1/12,000$ *cycles/hour* along the frequency axis. In the subtidal band, between 2 *hr* and 8 *hr* period, there are 4,501 spectral estimates. For twenty-five spectral estimates centred on frequency f_j with $Q = 100$, the misfit of (40) to spectral estimate s_i is

$$\epsilon_{ij} = A_j r_{ij} - s_i. \quad (41)$$

The error energy of the fit is

$$I_j = \sum_{i=j-12}^{j+12} \epsilon_{ij}^2. \quad (42)$$

Minimizing the error energy of the fit gives

$$A_j = \sum_{i=j-12}^{j+12} r_{ij} s_i / \sum_{i=j-12}^{j+12} r_{ij}^2, \quad (43)$$

with minimum error energy

$$I_{min} = \sum_{i=j-12}^{j+12} s_i^2 - A_j^2 \sum_{i=j-12}^{j+12} r_{ij}^2. \quad (44)$$

As a measure of the strength of a potential resonance of the form (40), we use the parameter $S_j^2 = A_j^2 / I_{min}$. When a large well-fit resonance is found, we expect S_j^2 to be large, and if a small, poorly fit spectral feature is found, we expect S_j^2 to be small. For each of the available 4,477 frequencies, f_j , in the subtidal band, we set $T_0 = 1/f_j$ and compute $f_R = 1/T_R$, $f_C = 1/T_C$ and $f_P = -1/T_P$ from equation (33). The values of S_R^2 , S_C^2 and S_P^2 of the resonance parameter S^2 at the discrete frequencies nearest f_R , f_C and f_P , respectively, are then multiplied together to form the splitting product P_j as an indicator of the presence of correctly split resonances. We show the resulting probability density function (PDF) for the splitting product computed at 4,119 points along the frequency axis in the subtidal band in Figure 4.

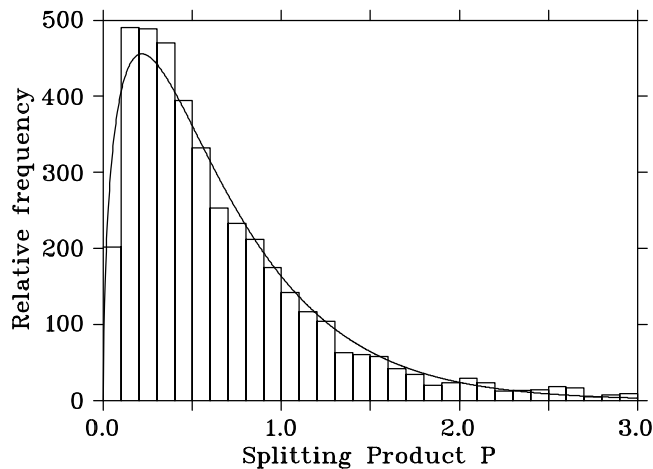


Figure 4: Probability density function (PDF) for the splitting product P . Bins in P are 0.1 wide. The fitted PDF is for a χ_ν^2 distribution with $\nu = 2.97614$ for the random variable $4.5314P$.

The PDF shown in Figure 4 allows the evaluation of the significance of translational triplets along the frequency axis. In Figure 5 we show the splitting products found between 2 hr and 10 hr periods. A very large value of P is found at $T_0 = 3.7975$ hr. From the PDF it is found that the probability of a realization of P_j larger than the largest shown in Figure 5 is only 1 in 6.8×10^{38} ! The resonances shown in Figure 3 seem to have been correctly identified as translational modes.

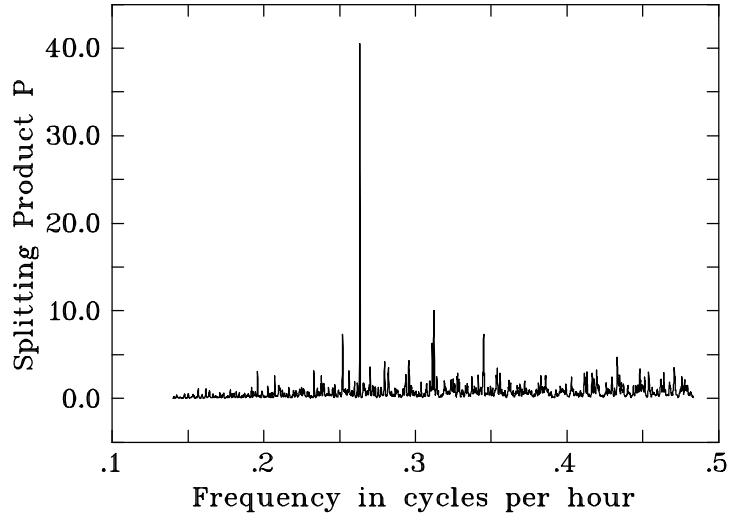


Figure 5: Splitting product P as a function of frequency. The large spike at $T_0 = 3.7975$ corresponds to the translational triplet plotted in Figure 3.

Plots of the splitting law for the three translational modes are shown in Figure 6. *The inviscid periods for the four Earth models plotted in this Figure are listed in Table 2.*

Table 2: Inviscid periods for the four Earth models shown plotted in Figure 6.

Periods	Retrograde (hours)	Axial (hours)	Prograde (hours)
Core11 Periods	5.1280	5.7412	6.5114
PREM Periods	4.6776	5.1814	5.7991
1066A Periods	4.0491	4.4199	4.8603
Cal8 Periods	3.5168	3.7926	4.1118

Two independent measures of viscosity are given, as the reduction in rotational splitting is larger for the retrograde mode than for the prograde equatorial mode. The retrograde equatorial mode gives $1.190 \pm 0.035 \times 10^{11} \text{ Pa}\cdot\text{s}$, while the prograde equatorial mode gives $1.304 \pm 0.034 \times 10^{11} \text{ Pa}\cdot\text{s}$. A balanced error value of $1.247 \times 10^{11} \text{ Pa}\cdot\text{s}$ yields viscous periods that are only 6.5 s longer than the observed periods.

From Figure 6, we see that the observed periods are close to those for the Cal8 Earth model. In Table 3 a detailed comparison of the Cal8 periods and those observed is shown.

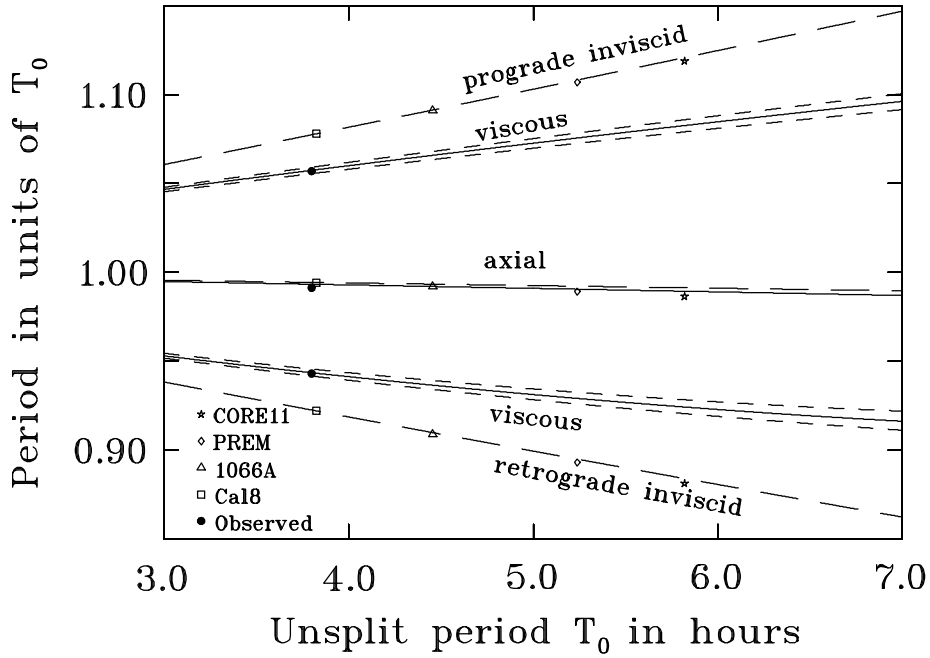


Figure 6: Splitting curves for the three translational modes. The inviscid curves are shown dashed using the splitting parameters for Earth model Cal8 (open squares) of Bolt and Uhrhammer (Bullen and Bolt, 1985, Appendix). Inviscid periods are over plotted for Earth models Core11 (open stars) (Widmer et al., 1988), PREM (open diamonds) (Dziewonski and Anderson, 1981) and 1066A (open triangles) (Gilbert and Dziewonski, 1975). Solid viscous splitting curves are for a single viscosity of $1.247 \times 10^{11} \text{ Pa} \cdot \text{s}$.

Table 3: Comparison of the observed translational mode periods with those of the Cal8 Earth model.

Periods	Retrograde (hours)	Axial (hours)	Prograde (hours)
Observed Periods	3.5822	3.7656	4.0150
Cal8 Viscous Periods	3.5840	3.7731	4.0168
Cal8 Inviscid Periods	3.5168	3.7926	4.1118

The close match of the observed periods to those of the Cal8 Earth model is due to the sensitivity of the translational mode periods to inner core density. In Figure 7, we show the density profiles of the Inner Core for Earth models Cal8, 1066A, PREM and Core11 together with their unsplit periods, T_0 .

The axial mode period suffers little rotational or viscous splitting. Its observed period provides a strict constraint on inner core density. The calculated axial mode period for Cal8 is only 27 s longer than the observed period. An overall density decrease in the inner core of only 2.25 milligrams $\cdot \text{cm}^{-3}$ would bring them into coincidence, giving a very strong confirmation of Cal8. In Table 4 we show a comparison of the unsplit period, T_0 , for the four Earth models with the observed value.

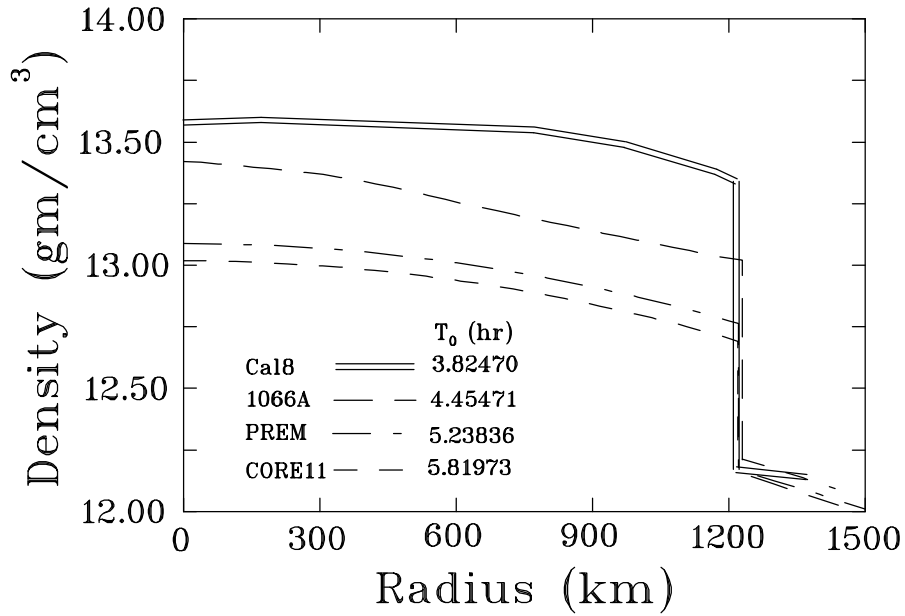


Figure 7: Detailed density profiles of the Inner Core for Earth models Cal8, 1066A, PREM and Core11. The range of $0.6 \text{ gm} \cdot \text{cm}^{-3}$ causes a nearly 2 hr difference in the unsplit period, T_0 , giving a resolution of $200 \text{ minutes}/\text{gm} \cdot \text{cm}^{-3}$.

Table 4: Comparison of the unsplit period, T_0 , for four Earth models with the observed value.

Earth Model	Unsplit Period T_0 (hrs.)	Deviation ΔT_0 (hrs.)	Error %
Observed	3.7985		
Cal8	3.82470	0.0262	0.69
1066A	4.45471	0.65621	17.28
PREM	5.23836	1.43986	37.91
Core11	5.81973	2.02123	53.21

4 A Viscosity Profile for the Outer Core

The boundary values of viscosity we have found are in very close agreement with an Arrhenius extrapolation of their laboratory experiments by Brazhkin (Brazhkin, 1998) and by Brazhkin and Lyapin (Brazhkin and Lyapin, 2000), who find $10^{11} \text{ Pa} \cdot \text{s}$ at the bottom of the outer core and $10^2 \text{ Pa} \cdot \text{s}$ at the top. We are prompted by the very close agreement of the viscosity measures at the boundaries with those provided by the Arrhenius extrapolation, to extend it to interpolate between the boundary values, to obtain a viscosity profile across the entire outer liquid core.

The Arrhenius description of the temperature and pressure dependence of the dynamic viscosity η is (Brazhkin, 1998)

$$\eta \sim \exp\left(\frac{E_{act_0} + PV_{act}}{kT}\right), \quad (45)$$

with E_{act_0} representing the activation energy at normal pressure, P the pressure, V_{act} the activation volume, k Boltzmann's constant and T the Kelvin temperature. V_{act} is proportional to the atomic volume, which, in turn, is inversely proportional to the density ρ . While the activation volume

for liquid metals at atmospheric pressure is very small, Brazhkin (1998) and Brazhkin and Lyapin (2000) report experimental results on pure iron at the melting temperature, T_m , that show it to be strongly pressure dependent up to pressures of 95 kbar. The strong pressure dependence requires integration of the differential form of the Arrhenius expression. For dominant pressure dependence, from expression (45) the differential increment in viscosity is proportional to

$$\frac{D}{\rho T_m} \exp D \frac{P}{\rho T_m} dP, \quad (46)$$

with D a pressure-dependent parameter, allowing for the pressure dependence of the activation volume, and dP being the differential increment in pressure. The integral of (46) over pressure is easily converted to an integral over radius r since $dP/dr = -\rho g$, where g is the gravitational acceleration at radius r . The viscosity at radius r is then

$$\eta(r) = \eta_b + \eta_b \int_b^r \frac{D}{\rho T_m} \exp\left(D \frac{P}{\rho T_m}\right) \frac{dP}{dr} dr, \quad (47)$$

with b the radius of the core-mantle boundary and $\eta_b = 2,371 \text{ Pa} \cdot \text{s}$ the dynamic viscosity at the top of the core. To perform the integration in (47), we require profiles of pressure, density, melting temperature and pressure gradient. The pressure profile can be found by integrating the product of gravity and density for an Earth model (we use Cal8, see Bullen and Bolt (1985), p.472). The melting temperatures are found by spline interpolation onto the Cal8 radii from those tabulated by Stacey (1992, p.459). The required profiles are shown in Table 5.

Table 5: Pressure, density, melting temperature and radial pressure gradient profiles.

radius (km)	P (10^{11} Pa)	ρ ($10^3 \text{ kg} \cdot \text{m}^{-3}$)	T_m (K)	dP/dr (10^4 Pa/m)
1,216	3.300	12.20	4,961	-5.600
1,371	3.223	12.14	4,905	-6.094
1,571	3.094	12.03	4,824	-6.737
1,821	2.916	11.84	4,710	-7.507
2,171	2.636	11.52	4,521	-8.479
2,571	2.278	11.11	4,258	-9.421
2,971	1.886	10.62	3,936	-10.12
3,171	1.681	10.33	3,751	-10.34
3,371	1.473	10.01	3,551	-10.47
3,486	1.350	9.860	3,429	-10.56

Since the activation volume increases strongly with pressure (Brazhkin, 1998) as represented by our parameter D in equation (46), we allow for a linear variation with depth through

$$D = D_b + \frac{b-r}{b-a} D_a, \quad (48)$$

where a is the radius of the inner core and D_b, D_a are constants. The integration in (47) is carried out by Simpson's rule over 100 steps with spline interpolation across the whole outer core. It is found that the constant, D_b , controls the curvature of the viscosity profile near the core-mantle

boundary, while the curvature otherwise departs only slightly from log-linear. Some numerical experimentation shows that the profile is closely log-linear, even near the core-mantle boundary, for a value $D_b = 4.5 \times 10^{-4} m^{-2} \cdot s^2 \cdot K$ and that for $D_a = 2.976 \times 10^{-3} m^{-2} \cdot s^2 \cdot K$, the viscosity at the bottom of the outer core, $\eta_a = 1.247 \times 10^{11} Pa \cdot s$, is closely matched. The resulting viscosity profile is shown in Figure 8.

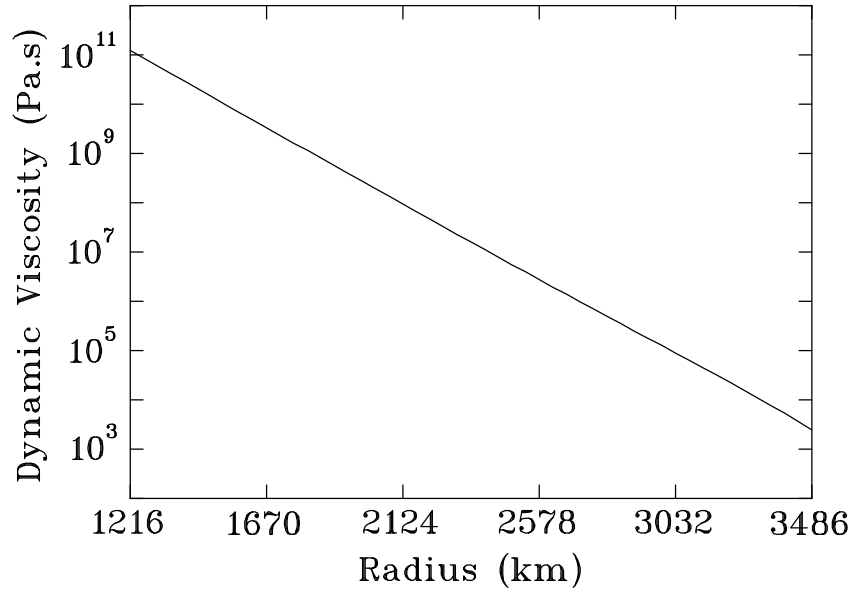


Figure 8: Viscosity profile for Earth's Outer Core.

5 Discussion

Given past uncertainties, the agreement between viscosities in the outer core measured from the VLBI observations of nutations, the superconducting gravimeter observations of the translational modes, and the Arrhenius extrapolation of laboratory high pressure and temperature experiments, is quite remarkable. The very large gap between direct observations and extrapolations of laboratory values appears to have closed. The viscosity values involved are for molecular viscosities and they are large enough that flows in the core are likely laminar in contradiction to conventional thought that the flows are turbulent and that the large viscosities reflect eddy viscosities.

According to the viscosity profile we have derived, the local Ekman number ranges from 1.2×10^{-2} at the bottom to 2.7×10^{-10} at the top of the outer core. Our results appear to confirm the suggestion by Braginsky (Braginsky, 1963) that the release of the latent heat of fusion as metallic constituents freeze out in the F-layer at the bottom of the outer core may be the energy source required to drive the geodynamo through compositional convection as studied by Loper and Roberts (Loper and Roberts, 1981). At the same time, except in the very lower part of the outer core, Ekman numbers are in the range 10^{-4} to 10^{-5} , or below, in which numerical dynamos operate (Olsen and Christiansen, 2002).

Acknowledgments

D.E.S. is grateful for financial support from the Natural Sciences and Engineering Research Council of Canada. We are indebted to Keith Aldridge for bringing the intricacies of Ekman layer theory to our attention.

References

- [1] Aldridge, K. D., 1967. An experimental study of axisymmetric inertial oscillations of a rotating liquid sphere. Ph.D. thesis, M. I. T., Cambridge, Massachusetts.
- [2] Aldridge, K. D., Toomre, A., 1969. Axisymmetric inertial oscillations of a fluid in a rotating spherical container. *J. Fluid Mech.* 37, pt. 2, 307-323.
- [3] Braginsky, S. I., 1963. Structure of the F layer and reasons for convection in the Earth's core. *Dokl. Akad. Nauk SSSR* 149, 8-10.
- [4] Brazhkin, V. V., Lyapin, A. G., 2000. Universal viscosity growth in metallic melts at megabar pressures: the vitreous state of the Earth's Inner Core. *Physics-Uspekhi* 43(5), 493-508.
- [5] Brazhkin, V. V. 1998. Investigation of the crystallization of liquid iron under pressure: extrapolation of the melt viscosity into the megabar range. *JETP Lett.* 68, 502-508.
- [6] Bullen, K. E., Bolt, B. A., 1985. *An Introduction to the Theory of Seismology*, 4th ed., Cambridge Univ. Press, Cambridge, UK, 499 pp.
- [7] Busse, F. H., 1968. Steady fluid flow in a precessing spheroidal shell. *J. Fluid Mech.* 33, 739-751.

- [8] Crossley, D., 1993. Eigensolutions and seismic excitation of the Slichter mode triplet for a fully rotating earth model. *EOS* 73(43), 60.
- [9] Crossley, D., Rochester, M., Peng, Z., 2007. Slichter modes and love numbers. *Geophys. Res. Lett.* 19, 1679-1682.
- [10] Courtier, N., Ducarme, B., Goodkind, J., Hinderer, J., Imanishi, Y., Seama, N., Sun, H., Merriam, J., Bengert, B., Smylie, D., 2000. Global superconducting gravimeter observations and the search for the translational modes of the inner core. *Phys. Earth Planet. Inter.* 117, 3-20.
- [11] Davis, R. G., Whaler, K. A., 1997. The 1969 geomagnetic impulse and spin-up of the Earth's liquid core. *Phys. Earth Planet. Inter.* 103, 181-194.
- [12] Dobson, D. P., 2002. Self-diffusion in liquid Fe at high pressure. *Phys. Earth Planet. Inter.* 139, 271-284.
- [13] Dziewonski, A. M., Anderson, D. L., 1981. Preliminary reference Earth model. *Phys. Earth Planet. Inter.* 25, 297-356.
- [14] Garland, G. D., 1971. *Introduction to Geophysics*. Saunders, Toronto, Canada, 420 pp.
- [15] Gilbert, F., Dziewonski, A. M., 1975. An application of normal mode theory to the retrieval of structural parameters and source mechanisms from seismic spectra. *Phil. Trans. R. Soc. Lond., A*, 278, 187-269.
- [16] Greenspan, H. P., 1969. *The theory of rotating fluids*. Cambridge Univ. Press, Cambridge, UK, 328pp.
- [17] Hinderer, J., Crossley, D., Jensen, O., 1995. A search for the Slichter triplet in superconducting gravimeter data. *Phys. Earth Planet. Inter.* 90, 183-195.
- [18] Jeffreys, H., 1926. The rigidity of Earth's central core. *Mon. Not. R. astr. Soc., Geophys. Suppl.* 1, 371-383.
- [19] Jiang, Xianhua 1993. *Wobble-Nutation Modes of the Earth*, Ph.D. thesis, York University, Toronto, Canada.
- [20] Jiang, Xianhua, Smylie, D. E., 1995. A search for free core nutation modes in VLBI nutation observations. *Phys. Earth Planet. Inter.* 90, 91-100.
- [21] Jiang, Xianhua, Smylie, D. E., 1966. Variational calculation of the free core nutation mode. *Phys. Earth Planet. Inter.* 94, 159-182.
- [22] Johnson, I. M., Smylie, D. E., 1977. A variational approach to whole-Earth dynamics. *Geophys. J. R. astr. Soc.* 50, 35-54.
- [23] Kroner, C., Jahr, Th. Jentsch, G., 2004. Results from 44 months of observations with a superconducting gravimeter at Moxa/Germany. *J. Geodyn.* 38, 263-280.
- [24] Loper, D. E., Roberts, P. H., 1981. A study of conditions at the inner core boundary of the Earth. *Annu. Rev. Earth Planet. Sci.* 18, 357-386.

- [25] Lumb, L. I., Aldridge, K. D., 1991. On viscosity estimates for the Earth's fluid Outer Core and Core-Mantle coupling. *J. Geomag. Geoelectr.* 43, 93-110.
- [26] Mathews, P. M., Buffett, B. A., Herring, T. A., Shapiro, I. I., 1991. Forced nutations of the earth: Influence of inner core dynamics, 1. Theory. *J. Geophys. Res.*, 96(B5), 8219-8242.
- [27] Moore, D. W., 1978. Homogeneous Fluids in Rotation. In: Roberts, P. H., Soward, A. M. (Eds.), *Rotating Fluids in Geophysics*, Academic Press, New York.
- [28] Olsen, P., Christensen, U. R., 2002. The time-averaged magnetic field in numerical dynamos with non-uniform boundary heat flow. *Geophys. J. Int.* 151, 809-823.
- [29] Pagiatakis, S. D., Yin, Hui, El-Gelil, M., 2007. Least-squares self-coherency analysis of superconducting gravimeter records in search for the Slichter triplet. *Phys. Earth Planet. Inter.* 160, 108-123.
- [30] Palmer, A., Smylie, D. E., 2005. VLBI observations of Free Core Nutations and viscosity at the top of the core. *Phys. Earth Planet. Inter.* 148, 285-301.
- [31] Poirier, J. P., 1988. Transport properties of liquid metals and viscosity of the Earth's core. *Geophys. J. Int.* 92, 99-105.
- [32] Rieutord, M., 2002. Slichter modes of the earth revisited. *Phys. Earth Planet. Inter.* 131, 269-278.
- [33] Roberts, P. H., Stewartson, K., 1965. On the motion of a liquid in a spheroidal cavity of a precessing rigid body, II. *Proc. Camb. Phil. Soc.* 61, 279-288.
- [34] Rogister, Y., 2003. Splitting of seismic-free oscillations and of the Slichter triplet using the normal mode theory of a rotating, ellipsoidal earth. *Phys. Earth Planet. Inter.* 140, 169-182.
- [35] Rosat, S., Rogister, Y., Crossley, D., Hinderer, J., 2006. A search for the Slichter triplet with superconducting gravimeters: impact of the density jump at the inner core boundary. *J. Geodyn.* 41, 296-306.
- [36] Rutter, M. D., R. A. Secco, H. Liu, T. Uchida, M. L. Rivers, S. R. Sutton and Y. Wang 2002. Viscosity of liquid Fe at high pressure. *Phys. Rev. B* 66, 060102-1-060102-4.
- [37] Smylie, D. E., Jiang, Xianhua, Brennan, B. J., Sato, K., 1992. Numerical calculation of modes of oscillation of the Earth's core. *Geophys. J. Int.* 108, 465-490.
- [38] Smylie, D. E., Jiang, Xianhua, 1993. Core oscillations and their detection in superconducting gravimeter records. *J. Geomag. Geoelectr.* 45, 1347-1369.
- [39] Smylie, D. E., Hinderer, J., Richter, B., Ducarme, B., 1993. The Product Spectra of gravity and barometric pressure in Europe. *Phys. Earth Planet. Inter.*, 80, 135-157.
- [40] Smylie, D. E., McMillan, D. G., 1998. Viscous and rotational splitting of the translational oscillations of Earth's solid inner core. *Phys. Earth Planet. Inter.* 106, 1-18.
- [41] Smylie, D. E., 1999. Viscosity near Earth's solid inner core. *Science.* 284, 461-463.

- [42] Smylie, D. E., McMillan, D. G., 2000. The inner core as a dynamic viscometer. *Phys. Earth Planet. Inter.* 117, 71-79.
- [43] Smylie, D. E., Francis, O., Merriam, J. B., 2001. Beyond tides - determination of core properties from superconducting gravimeter observations. *J. Geod. Soc. Jpn.* 47, 364-372.
- [44] Stacey, F. D., 1992. *Physics of the Earth*, 3rd. ed., Brookfield Press, Brisbane, Australia, 513 pp.
- [45] Stewartson, K., Roberts, P. H., 1963. On the motion of a liquid in a spheroidal cavity of a precessing rigid body. *J. Fluid Mech.* 17, 1-20.
- [46] de Vries, D., Wahr, J., 1991. The effects of the Earth's solid inner core and nonhydrostatic structure on the Earth's forced nutations and Earth tides. *J. Geophys. Res.* 96, 8275-8293.
- [47] Widmer, R., Masters, G., Gilbert, F., 1988. The spherical Earth revisited. 17th International Conference on Mathematical Geophysics, June 1988, Blanes, Spain, IUGG.

Appendix A

Ekman Boundary Layers and Dissipation

In this Appendix, we describe in detail the solution of the boundary layer equations (7) and the calculation of the rates of energy dissipation in the two boundary layers at the boundaries of the outer core. For convenience in keeping track of phase, the velocity components (v_θ, v_ϕ) will be taken to be complex phasors with time and longitude variations given by $e^{-i(\phi+\Omega t)}$. For an assumed radial dependence proportional to $e^{\lambda r}$, we are lead to the homogeneous system of equations

$$\begin{pmatrix} \lambda^2 \nu + i\Omega & 2\Omega \cos \theta \\ -2\Omega \cos \theta & \lambda^2 \nu + i\Omega \end{pmatrix} \begin{pmatrix} v_\theta \\ v_\phi \end{pmatrix} = 0. \quad (49)$$

For this system to have a solution, λ must satisfy

$$(\lambda^2 \nu + i\Omega)^2 = -4\Omega^2 \cos^2 \theta. \quad (50)$$

Thus,

$$\lambda^2 \nu + i\Omega = \pm i2\Omega \cos \theta. \quad (51)$$

Substitution of relation (51) into the system of equations (49), gives

$$v_\phi = \mp i v_\theta, \quad (52)$$

and

$$v_\phi = \pm i v_\theta. \quad (53)$$

The boundary layers are characterized by the dimensionless Ekman number

$$E_k = \frac{\nu}{b^2 \Omega}, \quad (54)$$

with length scale fixed by the radius b of the CMB. The four roots of the secular equation (50) are $\pm\lambda_1, \pm\lambda_2$ with

$$\lambda_1 = \frac{1-i}{b} \sqrt{\frac{1/2 + \cos \theta}{E_k}} = \frac{1+i}{\delta_1} \quad \text{for } \theta < 2\pi/3 \quad (55)$$

$$= \frac{1+i}{b} \sqrt{\frac{-1/2 - \cos \theta}{E_k}} = \frac{1+i}{\delta_1} \quad \text{for } \theta > 2\pi/3 \quad (56)$$

and

$$\lambda_2 = \frac{1-i}{b} \sqrt{\frac{1/2 - \cos \theta}{E_k}} = \frac{1-i}{\delta_2} \quad \text{for } \theta > \pi/3 \quad (57)$$

$$= \frac{1+i}{b} \sqrt{\frac{-1/2 + \cos \theta}{E_k}} = \frac{1+i}{\delta_2} \quad \text{for } \theta < \pi/3, \quad (58)$$

with δ_1, δ_2 , the respective boundary layer thicknesses, both of $O(\sqrt{E_k})$.

In the boundary layer near the top of the core, the perturbing velocity components (v_θ, v_ϕ) vanish with decreasing radius and increase with radius, so that at $r = b$, they are equal and opposite to

the interior nutation velocity components (6) to satisfy the no-slip condition at the CMB. Thus, the admissible values of λ satisfying equation (51) are λ_1, λ_2 . In the boundary layer near the bottom of the outer core, the perturbing velocity components vanish with increasing radius and increase with decreasing radius to satisfy the no-slip condition at the ICB. There, the admissible values of λ satisfying equation (51) are $-\lambda_1, -\lambda_2$. The perturbing velocity components are then given by the linear combinations

$$v_\theta = e^{-\Delta r/\delta_1} \left(f e^{i(\Delta r/\delta_1 \pm \phi \pm \Omega t)} \right) + e^{-\Delta r/\delta_2} \left(g e^{i(\Delta r/\delta_2 \pm \phi \pm \Omega t)} \right) \quad (59)$$

$$v_\phi = e^{-\Delta r/\delta_1} \left(i f e^{i(\Delta r/\delta_1 \pm \phi \pm \Omega t)} \right) - e^{-\Delta r/\delta_2} \left(i g e^{i(\Delta r/\delta_2 \pm \phi \pm \Omega t)} \right), \quad (60)$$

where the lower signs apply for the range $\pi/3 < \theta < 2\pi/3$, while the upper signs apply for the range $0 < \theta < \pi/3$ for terms involving δ_2 , and the upper signs apply for the range $2\pi/3 < \theta < \pi$ for terms involving δ_1 . Δr is the increment in radius. At the top of the core $\Delta r = b - r$, and at the bottom of the outer core $\Delta r = r - a$. In general, the linear combination coefficients are complex with real and imaginary parts expressed by

$$f = \alpha + i\beta \quad (61)$$

$$g = \gamma + i\epsilon. \quad (62)$$

Both the real and imaginary parts of expressions (59) and (60) are solutions of the boundary layer equations (7). Our interest is in the real parts of the velocity components given by

$$\begin{aligned} Rlv_\theta = & e^{-\Delta r/\delta_1} \left[\left(\alpha \cos \frac{\Delta r}{\delta_1} \pm \beta \sin \frac{\Delta r}{\delta_1} \right) \cos(\phi + \Omega t) \right. \\ & \left. + \left(\beta \cos \frac{\Delta r}{\delta_1} \mp \alpha \sin \frac{\Delta r}{\delta_1} \right) \sin(\phi + \Omega t) \right] \\ & + e^{-\Delta r/\delta_2} \left[\left(\gamma \cos \frac{\Delta r}{\delta_2} \pm \epsilon \sin \frac{\Delta r}{\delta_2} \right) \cos(\phi + \Omega t) \right. \\ & \left. + \left(\epsilon \cos \frac{\Delta r}{\delta_2} \mp \gamma \sin \frac{\Delta r}{\delta_2} \right) \sin(\phi + \Omega t) \right], \end{aligned} \quad (63)$$

$$\begin{aligned} Rlv_\phi = & e^{-\Delta r/\delta_1} \left[\left(-\beta \cos \frac{\Delta r}{\delta_1} \pm \alpha \sin \frac{\Delta r}{\delta_1} \right) \cos(\phi + \Omega t) \right. \\ & \left. + \left(\alpha \cos \frac{\Delta r}{\delta_1} \pm \beta \sin \frac{\Delta r}{\delta_1} \right) \sin(\phi + \Omega t) \right] \\ & + e^{-\Delta r/\delta_2} \left[\left(\epsilon \cos \frac{\Delta r}{\delta_2} \mp \gamma \sin \frac{\Delta r}{\delta_2} \right) \cos(\phi + \Omega t) \right. \\ & \left. + \left(-\gamma \cos \frac{\Delta r}{\delta_2} \mp \epsilon \sin \frac{\Delta r}{\delta_2} \right) \sin(\phi + \Omega t) \right]. \end{aligned} \quad (64)$$

For the velocity components (63) and (64) to cancel the components of (6) at the boundaries, we have

$$Rlv_\theta = (\alpha + \gamma) \cos(\phi + \Omega t) + (\beta + \epsilon) \sin(\phi + \Omega t) = Ar_0 \sin(\phi + \Omega t), \quad (65)$$

$$Rlv_\phi = (\epsilon - \beta) \cos(\phi + \Omega t) + (\alpha - \gamma) \sin(\phi + \Omega t) = Ar_0 \cos \theta \cos(\phi + \Omega t), \quad (66)$$

where r_0 is the boundary radius. $r_0 = b$ at the top of the core and $r_0 = a$ at the bottom of the outer core. Then,

$$\beta = \frac{1}{2}Ar_0(1 - \cos \theta), \quad \epsilon = \frac{1}{2}Ar_0(1 + \cos \theta), \quad \alpha = \gamma = 0. \quad (67)$$

Differentiation of expressions (63) and (64) yields the derivatives of the velocity components at the top of the core,

$$\frac{\partial Rlv_\theta}{\partial r} = \left(\mp \frac{\beta}{\delta_1} \mp \frac{\epsilon}{\delta_2} \right) \cos(\phi + \Omega t) + \left(\frac{\beta}{\delta_1} + \frac{\epsilon}{\delta_2} \right) \sin(\phi + \Omega t), \quad (68)$$

$$\frac{\partial Rlv_\phi}{\partial r} = \left(-\frac{\beta}{\delta_1} + \frac{\epsilon}{\delta_2} \right) \cos(\phi + \Omega t) + \left(\mp \frac{\beta}{\delta_1} \pm \frac{\epsilon}{\delta_2} \right) \sin(\phi + \Omega t), \quad (69)$$

while those at the bottom of the outer core are the negatives of these. At the top of the core, the leading order stresses on the outer surface are

$$\sigma_{r\theta} = \eta \frac{\partial Rlv_\theta}{\partial r} \quad \text{and} \quad \sigma_{r\phi} = \eta \frac{\partial Rlv_\phi}{\partial r}, \quad (70)$$

where η is the dynamic viscosity. At the bottom of the outer core, the leading order stresses on the inner surface are the negatives of these, so that on both surfaces the rate of dissipation of energy per unit area in the motion with velocity (6) against these stresses is

$$\begin{aligned} \frac{de}{dr} &= v_\theta \sigma_{r\theta} + v_\phi \sigma_{r\phi} \\ &= Ar_0 \eta \left[\left(\mp \frac{\beta}{\delta_1} \mp \frac{\epsilon}{\delta_2} \right) \cos(\phi + \Omega t) \sin(\phi + \Omega t) + \left(\frac{\beta}{\delta_1} + \frac{\epsilon}{\delta_2} \right) \sin^2(\phi + \Omega t) \right. \\ &\quad \left. + \cos \theta \left[\left(\frac{\epsilon}{\delta_2} - \frac{\beta}{\delta_1} \right) \cos^2(\phi + \Omega t) + \left(\mp \frac{\beta}{\delta_1} \pm \frac{\epsilon}{\delta_2} \right) \cos(\phi + \Omega t) \sin(\phi + \Omega t) \right] \right]. \end{aligned} \quad (71)$$

Substitution from (67), (55), (56), (57) and (58) yields, for $0 < \theta < \pi/3$,

$$\begin{aligned} \frac{de}{dt} &= \frac{1}{2} \rho_0 A^2 r_0^2 \left[\sqrt{v\Omega(1/2 + \cos \theta)} \right. \\ &\quad \left\{ \sin^2 \theta \left(\cos(\phi + \Omega t) \sin(\phi + \Omega t) - \cos^2(\phi + \Omega t) \right) + 1 - \cos \theta \right\} \\ &\quad - \sqrt{v\Omega(-1/2 + \cos \theta)} \\ &\quad \left. \left\{ \sin^2 \theta \left(\cos(\phi + \Omega t) \sin(\phi + \Omega t) + \cos^2(\phi + \Omega t) \right) - 1 - \cos \theta \right\} \right], \end{aligned} \quad (72)$$

and for $\pi/3 < \theta < 2\pi/3$,

$$\begin{aligned} \frac{de}{dt} &= \frac{1}{2} \rho_0 A^2 r_0^2 \left[\sqrt{v\Omega(1/2 + \cos \theta)} \right. \\ &\quad \left\{ \sin^2 \theta \left(\cos(\phi + \Omega t) \sin(\phi + \Omega t) - \cos^2(\phi + \Omega t) \right) + 1 - \cos \theta \right\} \\ &\quad + \sqrt{v\Omega(1/2 - \cos \theta)} \\ &\quad \left. \left\{ \sin^2 \theta \left(\cos(\phi + \Omega t) \sin(\phi + \Omega t) - \cos^2(\phi + \Omega t) \right) + 1 + \cos \theta \right\} \right], \end{aligned} \quad (73)$$

and for $2\pi/3 < \theta < \pi$,

$$\begin{aligned} \frac{de}{dt} = & \frac{1}{2} \rho_0 A^2 r_0^2 \left[-\sqrt{\nu\Omega} (-1/2 - \cos\theta) \right. \\ & \left. \left\{ \sin^2\theta \left(\cos(\phi + \Omega t) \sin(\phi + \Omega t) + \cos^2(\phi + \Omega t) \right) - 1 + \cos\theta \right\} \right. \\ & \left. + \sqrt{\nu\Omega} (1/2 - \cos\theta) \right. \\ & \left. \left\{ \sin^2\theta \left(\cos(\phi + \Omega t) \sin(\phi + \Omega t) - \cos^2(\phi + \Omega t) \right) + 1 + \cos\theta \right\} \right], \end{aligned} \quad (74)$$

with ρ_0 representing the density just inside the respective boundary.

Integrating over the entire boundary, the total rate of energy dissipation is

$$\begin{aligned} \frac{dE}{dt} = & r_0^2 \int_0^{2\pi} \int_0^\pi \frac{de}{dt} \sin\theta d\theta d\phi \\ = & -\frac{\pi}{2} \rho_0 A^2 r_0^4 \sqrt{\nu\Omega} \\ & \times \left[\int_0^{\pi/3} \sqrt{\frac{1}{2} + \cos\theta} \left(\sin\theta (1 - \cos\theta + \sin^2\theta) \right) d\theta \right. \\ & + \int_0^{\pi/3} \sqrt{-\frac{1}{2} + \cos\theta} \left(\sin\theta (1 + \cos\theta + \sin^2\theta) \right) d\theta \\ & + \int_{\pi/3}^{2\pi/3} \sqrt{\frac{1}{2} + \cos\theta} \left(\sin\theta (1 - \cos\theta + \sin^2\theta) \right) d\theta \\ & + \int_{\pi/3}^{2\pi/3} \sqrt{\frac{1}{2} - \cos\theta} \left(\sin\theta (1 + \cos\theta + \sin^2\theta) \right) d\theta \\ & + \int_{2\pi/3}^\pi \sqrt{-\frac{1}{2} - \cos\theta} \left(\sin\theta (1 - \cos\theta + \sin^2\theta) \right) d\theta \\ & \left. + \int_{2\pi/3}^\pi \sqrt{\frac{1}{2} - \cos\theta} \left(\sin\theta (1 + \cos\theta + \sin^2\theta) \right) d\theta \right], \end{aligned} \quad (75)$$

where, in the integration over ϕ , we have made use of the integrals

$$\int_0^{2\pi} \cos(\phi + \Omega t) \sin(\phi + \Omega t) d\phi = \frac{1}{2} \int_0^{2\pi} \sin\{2(\phi + \Omega t)\} d\phi = 0, \quad (76)$$

and

$$\int_0^{2\pi} \cos^2(\phi + \Omega t) d\phi = \frac{1}{2} \int_0^{2\pi} (\cos\{2(\phi + \Omega t)\} + 1) d\phi = \pi. \quad (77)$$

We may write (75) in the shorthand

$$\frac{dE}{dt} = -\frac{\pi}{2} \rho_0 A^2 r_0^4 \sqrt{\nu\Omega} [J_1 + J_2 + J_3 + J_4 + J_5 + J_6], \quad (78)$$

with $J_1, J_2, J_3, J_4, J_5, J_6$ representing the six integrals in (75). Evaluation of the integrals in expres-

sion (75) depends on the indefinite integrals

$$\begin{aligned}
I_1 &= \int \left(\frac{s}{2} \mp \cos \theta\right)^{1/2} \sin^3 \theta d\theta \\
&= \pm \frac{2}{3} \left(\frac{s}{2} \mp \cos \theta\right)^{3/2} \sin^2 \theta - \frac{8}{15} \left(\frac{s}{2} \mp \cos \theta\right)^{5/2} \cos \theta \mp \frac{16}{105} \left(\frac{s}{2} \mp \cos \theta\right)^{7/2}, \quad (79)
\end{aligned}$$

$$\begin{aligned}
I_2 &= \int \left(\frac{s}{2} \mp \cos \theta\right)^{1/2} (1 - \cos \theta) \sin \theta d\theta \\
&= \pm \frac{2}{3} \left(\frac{s}{2} \mp \cos \theta\right)^{3/2} \mp \frac{2}{3} \left(\frac{s}{2} \mp \cos \theta\right)^{3/2} \cos \theta - \frac{4}{15} \left(\frac{s}{2} \mp \cos \theta\right)^{5/2}, \quad (80)
\end{aligned}$$

$$\begin{aligned}
I_3 &= \int \left(\frac{s}{2} \mp \cos \theta\right)^{1/2} (1 + \cos \theta) \sin \theta d\theta \\
&= \pm \frac{2}{3} \left(\frac{s}{2} \mp \cos \theta\right)^{3/2} \pm \frac{2}{3} \left(\frac{s}{2} \mp \cos \theta\right)^{3/2} \cos \theta + \frac{4}{15} \left(\frac{s}{2} \mp \cos \theta\right)^{5/2}, \quad (81)
\end{aligned}$$

s representing the sign, which can take on either the value $+1$, or the value -1 , throughout each expression. Using (79), (80) and (81), and inserting limits of integration, we find

$$J_1 = \frac{13}{30} + \frac{16}{105} - \frac{18}{35} \sqrt{\frac{3}{2}}, \quad J_2 = -\frac{57}{105} \sqrt{2}, \quad J_3 = -\frac{1}{6} - \frac{44}{105}, \quad (82)$$

$$J_4 = -\frac{1}{6} - \frac{44}{105} = J_3, \quad J_5 = -\frac{57}{105} \sqrt{2} = J_2, \quad J_6 = \frac{13}{30} + \frac{16}{105} - \frac{18}{35} \sqrt{\frac{3}{2}} = J_1. \quad (83)$$

The six integrals sum to

$$J_1 + J_2 + J_3 + J_4 + J_5 + J_6 = -2 \sqrt{2} (9 \sqrt{3} + 19) / 35. \quad (84)$$

Substituting this result in expression (78), we find the rate of energy dissipation in each of the respective boundary layers to be

$$\frac{dE}{dt} = \frac{\pi}{35} \rho_0 A^2 r_0^4 \sqrt{2\nu\Omega} (9 \sqrt{3} + 19). \quad (85)$$

Appendix B

Viscous Coupling to the Inner Core and Shell

From relation (11), it is apparent that the reciprocal of the overall quality factor cannot be less than the reciprocal of the effective quality factor arising from the boundary layer at the ICB. Because of the high viscosity there, the inner core is likely to be tightly coupled to outer core wobble. The nearly retrograde diurnal wobbles of the outer core, associated with the free core nutations, give rise to viscous torques exerted by the outer core on the inner core and shell.

The viscous torques exerted by the outer core at the boundaries are

$$\mathbf{\Gamma} = \int \mathbf{r} \times (\hat{\boldsymbol{\theta}}\sigma_{r\theta} + \hat{\boldsymbol{\phi}}\sigma_{r\phi}) dS = \int (-\hat{\boldsymbol{\theta}}r\sigma_{r\phi} + \hat{\boldsymbol{\phi}}r\sigma_{r\theta}) dS, \quad (86)$$

where the integral is over the respective boundary surface. The spherical polar unit vectors are related to the Cartesian unit vectors $(\hat{\mathbf{i}}, \hat{\mathbf{j}}, \hat{\mathbf{k}})$ by

$$\hat{\boldsymbol{\theta}} = \hat{\mathbf{i}} \cos \theta \cos \phi + \hat{\mathbf{j}} \cos \theta \sin \phi - \hat{\mathbf{k}} \sin \theta, \quad (87)$$

$$\hat{\boldsymbol{\phi}} = -\hat{\mathbf{i}} \sin \phi + \hat{\mathbf{j}} \cos \phi. \quad (88)$$

The Cartesian components of the viscous torques are then

$$\begin{aligned} \mathbf{\Gamma} = & \hat{\mathbf{i}}r_0^3 \int_0^{2\pi} \int_0^\pi \sin \theta (-\sigma_{r\phi} \cos \theta \cos \phi - \sigma_{r\theta} \sin \phi) d\theta d\phi \\ & + \hat{\mathbf{j}}r_0^3 \int_0^{2\pi} \int_0^\pi \sin \theta (-\sigma_{r\phi} \cos \theta \sin \phi + \sigma_{r\theta} \cos \phi) d\theta d\phi \\ & + \hat{\mathbf{k}}r_0^3 \int_0^{2\pi} \int_0^\pi \sigma_{r\phi} \sin^2 \theta d\theta d\phi. \end{aligned} \quad (89)$$

From the expressions (70) for the leading order stresses, the integrations over ϕ are seen to depend on the elementary integrals

$$\begin{aligned} \int_0^{2\pi} \cos(\phi + \Omega t) \cos \phi d\phi &= \pi \cos \Omega t, & \int_0^{2\pi} \sin(\phi + \Omega t) \cos \phi d\phi &= \pi \sin \Omega t, \\ \int_0^{2\pi} \cos(\phi + \Omega t) \sin \phi d\phi &= -\pi \sin \Omega t, & \int_0^{2\pi} \sin(\phi + \Omega t) \sin \phi d\phi &= \pi \cos \Omega t, \\ \int_0^{2\pi} \cos(\phi + \Omega t) d\phi &= \int_0^{2\pi} \sin(\phi + \Omega t) d\phi = 0. \end{aligned}$$

The latter two integrals ensure that the viscous torques have only equatorial Cartesian components, (Γ_x, Γ_y) , and writing $\tilde{\mathbf{\Gamma}} = \Gamma_x + i\Gamma_y$, we have

$$\begin{aligned} \tilde{\mathbf{\Gamma}} = & -\pi r_0^3 \eta e^{-i\Omega t} \int_0^\pi \left[\cos \theta \sin \theta \left(\frac{\beta}{\delta_1} - \frac{\epsilon}{\delta_2} \right) - \sin \theta \left(\frac{\beta}{\delta_1} + \frac{\epsilon}{\delta_2} \right) \right] d\theta \\ & + i\pi r_0^3 \eta e^{-i\Omega t} \int_0^\pi \left[\cos \theta \sin \theta \left(\mp \frac{\beta}{\delta_1} \pm \frac{\epsilon}{\delta_2} \right) + \sin \theta \left(\pm \frac{\beta}{\delta_1} \pm \frac{\epsilon}{\delta_2} \right) \right] d\theta. \end{aligned} \quad (90)$$

Substitution from equations (55), (56), (57), (58) and (67) shows that evaluation of the torque expression (90) depends on the integrals

$$\begin{aligned}
& \int \sqrt{\left(\frac{s}{2} \mp \cos \theta\right)} \cos \theta \sin \theta d\theta \\
&= \pm \frac{2}{3} \cos \theta \left(\frac{s}{2} \mp \cos \theta\right)^{3/2} + \frac{4}{15} \left(\frac{s}{2} \mp \cos \theta\right)^{5/2}, \\
& \int \sqrt{\left(\frac{s}{2} \mp \cos \theta\right)} \cos^2 \sin \theta d\theta \\
&= \pm \frac{2}{3} \left(\frac{s}{2} \mp \cos \theta\right)^{3/2} \cos^2 \theta + \frac{8}{15} \left(\frac{s}{2} \mp \cos \theta\right)^{5/2} \cos \theta \pm \frac{16}{105} \left(\frac{s}{2} \mp \cos \theta\right)^{7/2}, \\
& \int \sqrt{\left(\frac{s}{2} \mp \cos \theta\right)} \sin \theta d\theta = \pm \frac{2}{3} \left(\frac{s}{2} \mp \cos \theta\right)^{3/2},
\end{aligned} \tag{91}$$

where, again, s represents the sign, which can take on either the value $+1$, or the value -1 , throughout each expression.

The total viscous torque is made up of contributions from three zones of latitude. The contribution from the region $0 < \theta < \pi/3$ is

$$\begin{aligned}
\tilde{\Gamma}_{0 < \theta < \pi/3} &= -\pi \rho_0 A r_0^4 \sqrt{\nu \Omega} e^{-i\Omega t} \left[\frac{41}{140} - \frac{9}{35} \sqrt{\frac{3}{2}} - \frac{19}{35} \frac{1}{\sqrt{2}} \right. \\
&\quad \left. + i \left\{ -\frac{41}{140} + \frac{9}{35} \sqrt{\frac{3}{2}} - \frac{19}{35} \frac{1}{\sqrt{2}} \right\} \right],
\end{aligned} \tag{92}$$

while the contribution from the region $\pi/3 < \theta < 2\pi/3$ is

$$\tilde{\Gamma}_{\pi/3 < \theta < 2\pi/3} = -\pi \rho_0 A r_0^4 \sqrt{\nu \Omega} e^{-i\Omega t} \frac{41}{70} (-1 + i), \tag{93}$$

and that from the region $2\pi/3 < \theta < \pi$ is

$$\begin{aligned}
\tilde{\Gamma}_{2\pi/3 < \theta < \pi} &= -\pi \rho_0 A r_0^4 \sqrt{\nu \Omega} e^{-i\Omega t} \left[\frac{41}{140} - \frac{9}{35} \sqrt{\frac{3}{2}} - \frac{19}{35} \frac{1}{\sqrt{2}} \right. \\
&\quad \left. + i \left\{ -\frac{41}{140} + \frac{9}{35} \sqrt{\frac{3}{2}} - \frac{19}{35} \frac{1}{\sqrt{2}} \right\} \right].
\end{aligned} \tag{94}$$

The total viscous torque is then

$$\tilde{\Gamma} = \pi \rho_0 A r_0^4 \sqrt{\nu \Omega} e^{-i\Omega t} \frac{19}{35} \sqrt{2} \left[1 + i + \frac{9}{19} \sqrt{3} (1 - i) \right]. \tag{95}$$

Separating the torques from the two boundary layers, the outer core exerts the viscous torque

$$\tilde{\Gamma}_a = \pi \rho_0 (a) A_a a^4 \sqrt{\nu_a \Omega} e^{-i\Omega t} \frac{19}{35} \sqrt{2} \left[1 + i + \frac{9}{19} \sqrt{3} (1 - i) \right] \tag{96}$$

on the inner core, while it exerts the viscous torque

$$\tilde{\Gamma}_b = \pi\rho_0(b)A_b b^4 \sqrt{\nu_b\Omega} e^{-i\Omega t} \frac{19}{35} \sqrt{2} \left[1 + i + \frac{9}{19} \sqrt{3} (1 - i) \right] \quad (97)$$

on the shell.

The extra nearly diurnal retrograde wobble of the outer core compared to its boundaries, in complex phasor notation, is

$$\tilde{\omega} = \omega_1 + i\omega_2 = A e^{-i\Omega t}, \quad (98)$$

with wobble angular velocity $\boldsymbol{\omega} = (\omega_1, \omega_2)$. The rate at which the outer core does work against the viscous torques is

$$\frac{dE}{dt} = \boldsymbol{\Gamma} \cdot \boldsymbol{\omega} = \Gamma_1 \omega_1 + \Gamma_2 \omega_2 = \frac{1}{2} (\tilde{\omega} \tilde{\Gamma}^* + \tilde{\omega}^* \tilde{\Gamma}), \quad (99)$$

where the torque vector is $\boldsymbol{\Gamma} = (\Gamma_1, \Gamma_2)$, and where the superscript asterisk indicates the complex conjugate. From the torque expression (95), we find the rate of energy dissipation in the boundary layers to be

$$\frac{dE}{dt} = \frac{\pi}{35} \rho_0 A^2 r_0^4 \sqrt{2\nu\Omega} (9\sqrt{3} + 19), \quad (100)$$

in agreement with equation (85).

The expressions (96) and (97) for the viscous torques the outer core exerts on its boundaries may be abbreviated to

$$\tilde{\Gamma}_a = \gamma_a e^{-i\Omega t} A_a \quad (101)$$

and

$$\tilde{\Gamma}_b = \gamma_b e^{-i\Omega t} A_b, \quad (102)$$

where

$$\gamma_a = \pi\rho_0(a) a^4 \sqrt{\nu_a\Omega} \frac{19}{35} \sqrt{2} \left[1 + i + \frac{9}{19} \sqrt{3} (1 - i) \right] \quad (103)$$

and

$$\gamma_b = \pi\rho_0(b) b^4 \sqrt{\nu_b\Omega} \frac{19}{35} \sqrt{2} \left[1 + i + \frac{9}{19} \sqrt{3} (1 - i) \right]. \quad (104)$$